European Journal of Pharmaceutics and Biopharmaceutics 163 (2021) 252–265

Contents lists available at ScienceDirect

European Journal of Pharmaceutics and Biopharmaceutics

journal homepage: www.elsevier.com/locate/ejpb

Improved multidetector asymmetrical-flow field-flow fractionation method for particle sizing and concentration measurements of lipid-based nanocarriers for RNA delivery

R. Mildner [a], S. Hak [b], J. Parot [b], A. Hyldbakk [b], S.E. Borgos [b], D. Some [c], C. Johann [a], F. Caputo [b,*]

[a] Wyatt Technology, Hochstrasse 12a, 56307 Dernbach, Germany
[b] Department of Biotechnology and Nanomedicine, SINTEF Industry, Trondheim, Norway
[c] Wyatt Technology, 6330 Hollister Ave., Santa Barbara, CA 93117, USA

ARTICLE INFO

Keywords:
Lipid-based nanoparticles
RNA delivery
Asymmetric-flow field-flow fractionation
Particle size
Physical–chemical characterisation
Particle concentration
Frit-inlet channel
Nanomedicine

ABSTRACT

Lipid-based nanoparticles for RNA delivery (LNP-RNA) are revolutionizing the nanomedicine field, with one approved gene therapy formulation and two approved vaccines against COVID-19, as well as multiple ongoing clinical trials. As for other innovative nanopharmaceuticals (NPhs), the advancement of robust methods to assess their quality and safety profiles—in line with regulatory needs—is critical for facilitating their development and clinical translation. Asymmetric-flow field-flow fractionation coupled to multiple online optical detectors (MD-AF4) is considered a very versatile and robust approach for the physical characterisation of nanocarriers, and has been used successfully for measuring particle size, polydispersity and physical stability of lipid-based systems, including liposomes and solid lipid nanoparticles. However, the unique core structure of LNP-RNA, composed of ionizable lipids electrostatically complexed with RNA, and the relatively labile lipid-monolayer coating, is more prone to destabilization during focusing in MD-AF4 than previously characterised nanoparticles, resulting in particle aggregation and sample loss. Hence characterisation of LNP-RNA by MD-AF4 needs significant adaptation of the methods developed for liposomes. To improve the performance of MD-AF4 applied to LNP-RNA in a systematic and comprehensive manner, we have explored the use of the frit-inlet channel where, differently from the standard AF4 channel, the particles are relaxed hydrodynamically as they are injected. The absence of a focusing step minimizes contact between the particle and the membrane, reducing artefacts (e.g. sample loss, particle aggregation). Separation in a frit-inlet channel enables satisfactory reproducibility and acceptable sample recovery in the commercially available MD-AF4 instruments. In addition to slice-by-slice measurements of particle size, MD-AF4 also allows to determine particle concentration and the particle size distribution, demonstrating enhanced versatility beyond standard sizing measurements.

1. Introduction

The research focus in the field of pharmacology is rapidly shifting from therapeutics based on small molecules to large, complex drugs, so-called biologics. Biological drugs include, among others, nucleic acids such as small interfering and messenger RNA molecules (siRNA and

Abbreviations: aCSF, Artificial cerebrospinal fluid; AF4, Asymmetric-flow field-flow fractionation; BSA, Bovine serum albumin; CDI, Centre-Downstream Injection; COV, Coefficient of variation; CQAs, Critical quality attributes; DLS, Dynamic light scattering; DSPC, 1,2-distearoyl-*sn*-glycero-3-phosphocholine; EtOH, Ethanol; EUNCL, European Nanomedicine Characterisation Laboratory; FBS, Foetal Bovine Serum; FF, Focus flow; FI, Frit inlet; FDA, Food and Drug Administration; FWHM, Full width at half maximum; HS, Human Serum; LC, Long channel; LC-MS/MS, Liquid chromatography with tandem mass spectrometry; LNP-RNA, Lipid-based nanoparticles for nucleic acid delivery; MALS, Multiangle light scattering; MC3, Dilinoleylmethyl-4-dimethylaminobutyrate; MD-AF4, Multidetector asymmetric flow field flow fractionation; MeOH, Methanol; NCI-NCL, National Cancer Institute - Nanotechnology Characterization Laboratory; NP, Nanoparticles; NPhs, Nanopharmaceuticals; NTA, Nanoparticle tracking analysis; PBS, Phosphate Buffered Saline; PdI, Polydispersity index; PEG2000-DMG, 1,2-Dimyristoyl-*rac*-glycero-3-methoxypolyethylene glycol-2000; PSD, Particle size distribution; QELS, Quasi-elastic light scattering; Rg, Radius of gyration; Rh, Hydrodynamic radius; RI, Refractive index; RT, Room temperature; TEM, Transmission electron microscopy; TRPS, Tuneable resistive pulse sensing; UV–Vis, Ultraviolet–visible; XF, Crossflow.

* Corresponding author.
E-mail address: fanny.caputo@sintef.no (F. Caputo).

https://doi.org/10.1016/j.ejpb.2021.03.004
Received 3 November 2020; Received in revised form 9 February 2021; Accepted 11 March 2021
Available online 18 March 2021

mRNA, respectively) and the gene-editing CRISPR/Cas technology [1]. The potential of nucleic acid-based therapies to answer unmet clinical needs is almost endless. It includes anti-infective and cancer vaccines, immune activation, in-body production of patients' own therapeutic antibodies, protein replacement therapies, regenerative medicine – and conceivably permanent gene therapy of any genetic disorder by encoding gene editing complexes. This paradigm shift in pharmacology is, in turn, revolutionizing the field of nanomedicine and renewing the interest of the scientific community in nano-delivery systems. Nano-encapsulation has been the recent enabling technology to deliver nucleic acids to their intracellular site of action. It facilitates protection of the nucleic acid (active pharmaceutical ingredient, API) from degradation by endogenous nucleases in the blood stream and an increase in targeted delivery, improving safety and, notably, efficacy of the nucleic acid therapeutics [2–8]. Lipid-based nanoparticle (LNP) systems containing an ionizable lipid, which complexes the nucleic acids in the protective nanoparticle core (LNP-RNA), are unquestionably the front runners among the nano-delivery systems tested. In 2018, the Food and Drug Administration (FDA) approved the first siRNA therapy encapsulated in LNPs, patisiran (Onpattro®) by Alnylam Pharmaceuticals. Importantly, at the end of 2020-beginning of 2021 two vaccines against the ongoing COVID-19 pandemic, based on mRNA technology encapsulated in LNPs, were approved by regulatory authorities in USA, Europe, UK and other countries: BioNTech/Pfizer's tozinameran and Moderna's mRNA-1273. Additionally, numerous other LNP-RNA therapeutics are in the pipeline and advanced clinical trials [9].

The development of new pharmaceutical formulations with such unprecedented speed has increased the need for accurate and robust characterization strategies to assure their quality and safety according to regulatory needs. New regulatory guidance documents specifically focused on LNP-RNA are still to be developed. However, current guidelines for liposomes [10] could be a basis for identifying the critical quality attributes (CQAs) of the LNP-RNA drug products. These attributes may include, among others, particle size distribution (PSD) and polydispersity, physical and chemical stability, particle concentration, chemical composition and RNA sequence, RNA loading levels, and stability.

Asymmetric-flow field-flow fractionation (AF4) is a very powerful technique for the analysis of particle size, polydispersity and physical stability of nanopharmaceuticals (NPhs) in complex biological media [11–13], and also for assessing particle concentration [14,15]. Multiple studies have shown the versatility of MD-AF4 for the analysis of lipid-based drug-delivery systems, including liposomes and solid lipid nanoparticles [16–20]. However, methods validated on one specific lipid-based system may not be immediately transferable to all lipid-based nanocarriers, including the nano-delivery carriers specifically engineered for RNA delivery. In fact, the latter nano-formulations are multicomponent lipid systems containing an ionizable lipid, a phospholipid, cholesterol, and a PEG-lipid, that possess a very different structure from liposomes or solid lipid nanoparticles [21]. The ionizable lipids complex the RNA to form a core structure with helper lipids (phospholipid and cholesterol) enveloping the lipid–RNA complex, while the PEG-lipid stabilizes the nanoparticle in the aqueous dispersion.

Preliminary attempts to apply the method recently developed by Parot et al. for liposomes [17] and by Caputo et al for solid LNPs [19] to measure LNP-RNA were unsatisfactory, suggesting that focusing ionizable lipid/RNA complex structures in the AF4 channel may induce particle aggregation and destabilization. Those effects are deemed responsible for sample loss due to adsorption onto the semipermeable membrane that serves as the accumulation wall in AF4, and are not acceptable according to the technical specification ISO/TS 21362 "*Nanotechnologies — Analysis of nano-objects using asymmetrical-flow and centrifugal field-flow fractionation*" [22]. For this reason, in the present study, we investigate the use of a modified AF4 channel equipped with a frit inlet (FI), where the sample is relaxed hydrodynamically as it enters the channel. This is achieved by applying a frit-inlet flow, entering the channel from the top toward the bottom frit element, not far from the channel inlet. Since the frit-inlet flow is about 20 times faster than the channel flow (Fig. 1C) it generates a compressive force leading to hydrodynamic relaxation. The process is much gentler on the analyte than the focusing step required in the standard MD-AF4 configuration (Fig. 1A-B). The main advantage of the FI channel is, thus, the possibility to omit the focusing step and avoid membrane adsorption, as explained in section 1.1.

In the present study, we compare the performance of two types of AF4 separation channels: the standard AF4 long channel (LC) and the FI channel on the currently available instrumental platforms (from Wyatt Technology and from Postnova Analytics). The results enable the development and validation of a universal, robust method, possessing satisfactory reproducibility and acceptable sample recovery, as required by ISO/TS 21362 [22]. The standard operating procedure jointly developed by two state-of-the-art infrastructures in NPh characterisation, the European Nanomedicine Characterisation Laboratory (EUNCL) and the NCI-Nanotechnology Characterization Laboratory (NCI-NCL), is considered here as a starting point for method development and performing the necessary quality controls to assure reliable instrument performance on all the platforms tested [23,24].

As an additional objective, we apply MD-AF4 (in particular AF4-MALS) to measure the particle concentration and particle size distribution of lipid-based nanocarriers, supporting the results obtained by widely used techniques for particle concentration measurements such as nanoparticle tracking analysis (NTA). Overall, this work demonstrates the versatility of MD-AF4 in the characterisation and quality control of lipid-based nanocarriers, widening its applicability to innovative systems such as LNP-RNA.

1.1. MD-AF4 principle and frit inlet vs standard channel

The theory of AF4 as well as its versatility in the field of (nano) medicine have been reviewed by many authors [13,24–27]. AF4 separation is achieved by establishing a parabolic laminar flow profile of the carrier liquid in a thin channel, without the need for a stationary phase. For this reason, MD-AF4 is a very powerful tool for organic nanoparticles such as liposomes, lipid-based NPs, extracellular vesicles and polymeric particles commonly used in nanomedicine. The channel is delimited by an impermeable top layer (upper wall) and by a semipermeable membrane in its bottom part, known as the accumulation wall. Separation is obtained by applying a perpendicular field, the crossflow (XF), produced by flowing the carrier liquid towards and through the accumulation wall, with the aim to concentrate the injected particles towards the semipermeable membrane.

In a conventional LC, a relaxation/focusing phase is imposed prior to sample elution from the channel. During focusing, the sample is injected and concentrated in a thin band at one end of the channel by opposing flows from both channel ends (Fig. 1A-B, blue arrows). At the same time, the perpendicular focus flow (FF) drives particle concentration toward the accumulation wall, where the concentration gradient is counter-balanced by Brownian motion, which is faster for smaller particles. Two focusing modes are currently available in the market for LC technologies. In centre-downstream injection (CDI) mode (available on Wyatt's Eclipse AF4 and Eclipse NEON systems), the sample is injected via a separate port positioned near the focusing position and distinct from the main channel inlet (Fig. 1A). In tip-injection mode (Postnova's AF2000, Wyatt's Eclipse DualTec and Eclipse NEON systems) the sample and the carrier liquid are injected from the same port (tip port), and the sample migrates a few centimetres until reaching the focusing position (Fig. 1B). In the latter mode, higher interaction is expected between the particles and the membrane during focusing, due to more extended contact of the particles with the membrane.

After focusing, when the AF4 system is operating in the normal elution mode (relevant for particle sizes below ~ 1 μm), a dynamic

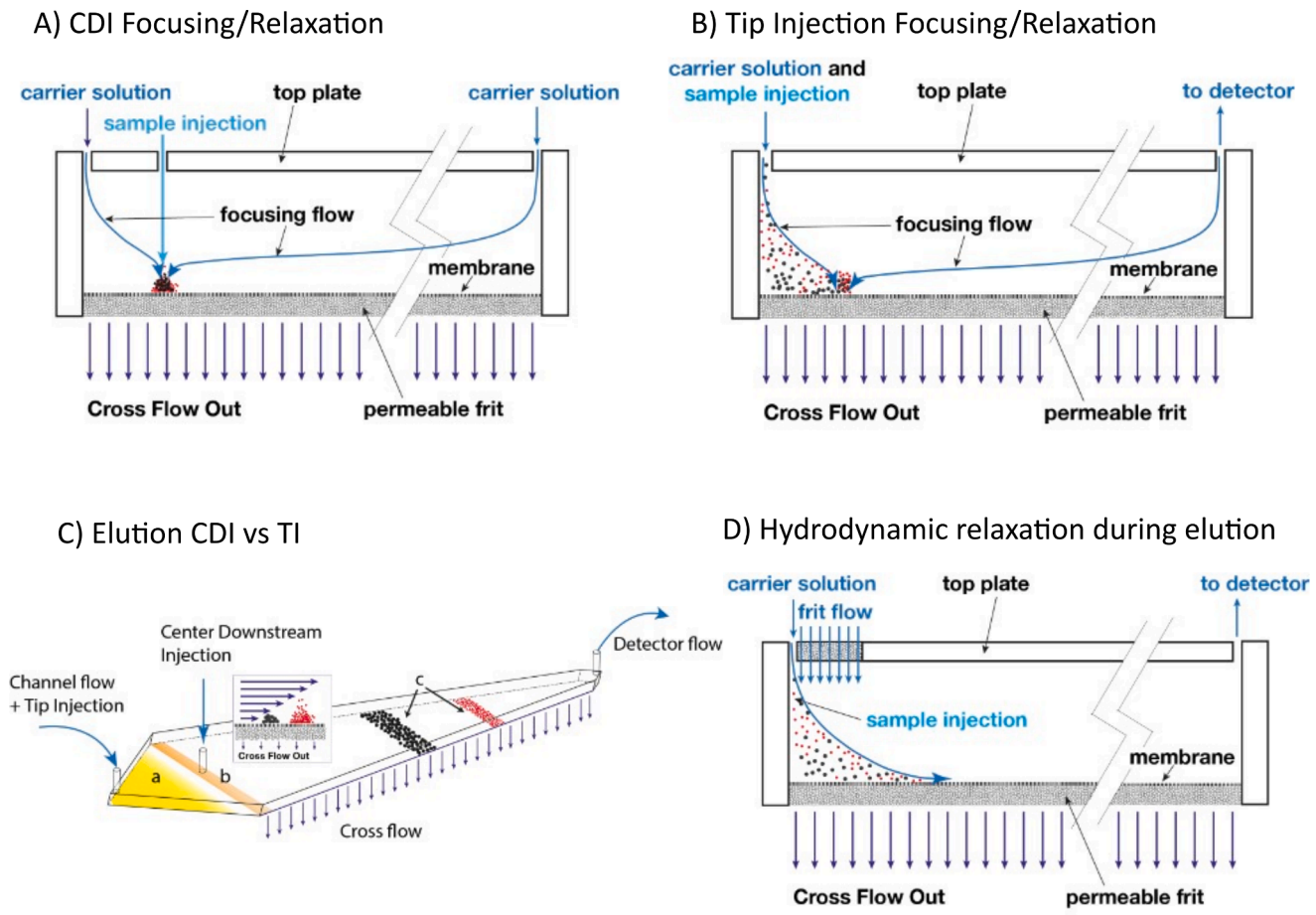

Fig. 1. Schematic representation of the three available focusing/relaxation in the normal elution operation mode. A) Centre-downstream injection (CDI) focusing/relaxation mode in the LC, where the sample is injected via a dedicated port in proximity to the focusing position; B) Tip-injection focusing/relaxation mode in the LC where the sample is injected from the same port as the carrier liquid (tip channel inlet) at the beginning of the channel and migrate to the focusing position during focusing, C) elution mode in LC, showing the migrating sample bands, where the smaller objects are faster D) FI channel mode, where there is no focusing step but the sample is injected during elution from the tip channel inlet and is hydrodynamically relaxed by a local crossflow, generated by the carrier liquid pushed through a porous FI (frit flow), that is about 20 times faster than the sample flow.

equilibrium is established (relaxation phase): smaller particles will, on average, be higher above the accumulation wall, while the larger ones will stay more in its proximity. The relative height above the accumulation wall is strictly in proportion to the particle's diffusion coefficient. Upon switching to the elution phase, wherein unidirectional channel flow is established from the channel inlet toward the channel outlet and detectors, a parabolic flow profile is formed inside the channel as shown in Fig. 1C. The flow profile leads to a differential migration velocity according to the average distance of the particles above the accumulation wall, corresponding in turn to their diffusion coefficient: smaller particles are eluted faster compared to larger particles. The amount of XF can be progressively reduced during elution, releasing particles of incrementally larger sizes, in order to speed up the separation process. This allows the separation of particles with a wide size distribution, e.g., an aggregate population with a much bigger size compared to the main fraction. It should be noted that this mode of operation (normal elution mode) does not apply to particles larger than roughly one micron, where elution order is reversed due to a different separation principle called steric/hyperlayer mode.

The focusing/relaxation step might, in some cases, cause a loss of sample due to adsorption on the accumulation wall (i.e. the membrane), while sample loss at the membrane is usually negligible once the elution mode has started [28]. Adsorption during focusing, resulting in low sample recoveries and unreliable measurements, can be avoided with an existing alternative, injection/relaxation with a FI channel. In an FI channel, the sample is introduced via the primary carrier stream flowing through the channel's tip inlet, while the secondary flow (the frit flow, FF) enters through a small frit element located in the top plate, which creates a local crossflow that is about 20 times faster than the sample flow and induces hydrodynamic relaxation of the sample (Fig. 1D). There is no transition between focusing and elution mode, and sample flow is directed from the tip to the end of the channel from the moment that sample injection starts.

The FI has been used for the analysis of bio-polymer systems, such as hyaluronic acid and pullulan, of polyion complexes self-assemblies and of proteins [29–33]. Despite being, in principle, a very interesting solution for many of the "soft" nanocarrier systems used in nanomedicine that suffer from aggregation and sample loss, such as virus-like particles, LNPs and exosomes, its potential is still largely unexplored.

1.2. The potential of using multiple detectors downstream of AF4 separation

Separation of nanoparticles is just the first stage in their characterization by MD-AF4. The ability to perform a variety of online measurements on the purified and nearly monodisperse fractions, flowing through one or more detectors, means that each species can be analysed thoroughly for physical and chemical properties with very high resolution.

Measurement of particle size is performed by multiple sizing

detectors such as dynamic light scattering (DLS) or multi-angle static light scattering (MALS), being a very useful tool to check batch-to-batch variability and sample stability during storage or in biological media [11]. By combining results obtained by both in-line MALS and DLS detection, the radius of gyration (R_g) and hydrodynamic radius (R_h), respectively, can be measured simultaneously. The two quantities can be combined to calculate the shape factor $\rho = R_g/R_h$ [12,13,22], which is an indirect indication of particle shape and particle morphology, e.g. indicating that uniform spheres or ellipsoids, hollow spherical shells, rods, etc are present in the samples [34].

MALS data can also be used to calculate particle concentration, provided that the shape, structure and refractive index (RI) of the sample and solvent are known and that sample recovery is acceptable. An algorithm from Wyatt Technology—described in US patent 6774994 and implemented in the current software version, ASTRA 7—enables calculation of the total particle number and concentration in any given fractogram range, as well as the overall PSD in relative units and on a logarithmic size scale. In the current work, an external macro combines the relative PSD and total particle number from ASTRA to obtain the absolute, number-based PSD in particles/nm or particles/mL/nm, on a linear size axis. The outcome, previously tested by the authors on liposomes and polystyrene nanoparticles, is comparable to results obtained by single-particle techniques such as NTA which are widely used for submicron particle concentration measurements [35,36].

Online measurements performed with concentration detectors like UV–Vis, inductively-coupled plasma-mass spectroscopy and/or RI detectors, can further enable evaluation of chemical composition and drug loading [13]. Individual fractions may be collected for further off-line analysis by e.g. transmission electron microscopy or mass spectrometry.

A major challenge in the characterization of LNP-RNA particles is determining the relative nucleic acid content of each size fraction. One approach is to collect size fractions after separation by AF4 and subsequently quantify the lipid and nucleic acid content of each fraction by standard analytical techniques such as reverse-phase liquid chromatography or real-time polymerase chain reaction (qPCR). This is a cumbersome process requiring significant time and labour and is limited by the size resolution of each fraction. Triple-detector online analysis of MALS, UV and RI signals is commonly used to characterize conjugated macromolecules such as glycoproteins and even adeno-associated viruses [34]. This method, known as conjugate analysis, provides the composition of a binary conjugate, in terms of the molar mass of each component in each eluting fraction, with no additional experimental effort. However, this method is generally not applicable to nanoparticles with radius above roughly 30 nm due to scattering in the UV detector. Recent algorithmic advances overcome the UV scattering issue and may be able to provide accurate analysis of larger particles such as LNP-RNA, determining the relative fraction of RNA and the number of RNA molecules in the particle as a function of particle size. The degree of accuracy and reliability of this method is currently under evaluation and will be the subject of a follow-up paper.

1.3. The importance of testing repeatability, reproducibility, and robustness: ISO/TS 21362

Acceptance of MD-AF4 measurements in a pharmaceutical production environment, as well as for regulatory purposes, requires demonstrating repeatability, reproducibility and robustness of the method, according to the harmonised guideline ICHQ2R1, selecting the criteria that are relevant to sizing measurements. In 2018, a first standard document focusing on field-flow fractionation techniques was published by ISO: the technical specification ISO/TS 21362 [22]. This document detailed, for the first time, the key criteria to consider during the development and validation of MD-AF4 analysis of nano-objects and their agglomerates or aggregates. Test conditions that enable reproducibility across laboratories are described, and guidance for method optimisation and validation is provided. Among the key criteria that a validated method must satisfy are the following two:

(a) percent recovery R% of the analyte after passing through the channel which should be higher than 70%, or, for performance separations (e.g. particle concentration measurements), above 90%;
(b) a relative standard uncertainty lower than 5% for retention time (peak maximum of the fractogram), R% and size measurements. Size values are to be reported either as the mode value or as the average size across the full-width half-maximum (FWHM), depending on sample polydispersity.

It was recently shown that those requirements can be satisfied in MD-AF4 measurements of liposomes [17]. In the present work we demonstrate that, by modifying and optimising the method validated for the analysis of liposome, it is possible to develop a robust and reproducible method that satisfies the criteria described in ISO/TS 21362, specifically applicable to the analysis of RNA-LNP formulations.

2. Experimental section

2.1. Reagents

Bovine serum albumin (BSA), monomer ≥ 97%, foetal bovine serum (FBS), phosphate buffered saline (PBS) tablets and 1,2-distearoyl-*sn*-glycero-3-phosphocholine (DSPC) were purchased from Sigma Aldrich. DSPC-d70 and Cholesterol standards were purchased from Avanti Polar. dilinoleylmethyl-4-dimethylaminobutyrate (Dlin-MC3-DMA or MC3) used in this work was donated by our collaborators from the University of Utrecht (Prof. Raymond Schiffelers). All the HPLC-grade solvents were purchased from Fluka or VWR. 1,2-dimyristoyl-*rac*-glycero-3-methoxypolyethylene glycol-2000 (PEG2000-DMG) was purchased from NOF. The siRNA was provided by Integrated DNA Technologies. Human serum (HS) was purchased from the local blood bank at St. Olavs University Hospital in Trondheim. Artificial cerebrospinal fluid (aCSF) was kindly provided by Alicja Molska from the Department of Circulation and Medical Imaging at NTNU in Trondheim. PBS and aCSF were filtered through 200 nm pore size filter membranes before use.

2.2. LNP synthesis

LNPs were synthesized using Nanoassembler (Precision Nanosystems). Stock solutions of cholesterol, DSPC, and PEG2000-DMG were prepared at 10 mg/mL in EtOH and of MC3 or C12-200 at 20 mg/mL for LNP1-RNA and LNP2-RNA respectively. Four batches using MC3 (LNP1-RNA samples) and one batch using C12-200 were synthetized to check for batch-to-batch variability and fine difference induced by using different ionizable lipids. Lipids were mixed at a molar ratio of 50:38.5:10:1.5 MC3(C12-200):cholesterol:DSPC:PEG2000-DMG and the EtOH volume was adjusted to obtain a 10 mM lipid concentration. The siRNA used had a molar mass of 13457.5 g/mol and was dissolved in RNase-free 25 mM acetate buffer of pH 4 to a concentration of 0.0132 mM. The 10 mM lipid mixture in EtOH and the siRNA solution in acetate buffer were mixed in a Nanoassembler at a 1:3 ratio resulting in a lipid to nucleic acid (N/P) ratio of 3 and an LNP formulation with 25 mol% EtOH, 2.5 mM lipid, and 133.5 mg/mL siRNA. To remove EtOH and potential non-encapsulated siRNA, and restore pH to 7.4, 1 mL of the formulation was dialysed (20000 Da MWCO membrane) overnight in the dark against 1 L of PBS at 4 °C.

2.3. siRNA content by RiboGreen assay

To measure the total siRNA concentration in the LNPs, we used the Quant-iT™ RiboGreen RNA Assay Kit (ThermoFisher Scientific). This assay is based on fluorescence enhancement of the dye RiboGreen upon binding to an RNA strand. Although the kit is not sequence specific, it is

very sensitive to RNA and can detect RNA down to 1 ng/mL, with a linear response from 1 ng/mL to 1 μg/mL. The excitation maximum for Quant-iT™ RiboGreen reagent, when bound to RNA, is $\lambda_{ex} = 500$ nm and the emission maximum is $\lambda_{em} = 525$ nm, and fluorescence was measured using these excitation and emission wavelengths. The assay was performed in a 96 well plate according to the manufacturer's manual with the following adaptations: Before adding 100 μL RiboGreen working solution to the samples, 50 μl 2% Triton 100-X in Tris-EDTA buffer was added to all standards and samples (sample volume: 50 μL) and incubated at 37 °C for 15 min to disrupt the LNPs and disperse the siRNA. An LNP formulation without siRNA was included to correct for background fluorescence originating from the lipids.

2.4. Total lipid content by LC-MS/MS:

The concentrations and the relative ratios of all the lipidic components were determined by liquid chromatography with mass spectrometry (LC-MS/MS).

Sample preparation: The LNPs and lipid stocks in EtOH were diluted in MeOH before analysis with LC-MS/MS. LNPs were diluted 40x, 200x, and 1000x, EtOH lipid stocks were diluted 500x, 1000x, 5000x, 10000x. The different LNP dilutions were used to assure that the concentrations in all samples for each of the lipids were within the calibration curve concentration range. Moreover, correspondence between the calculated concentrations from the different dilutions provided an additional quality check.

Instrument and methods: Table S1-S4 respectively provide details about the instruments used, the method used to measure MC3, Cholesterol, and DSPC, and the method used to quantify PEG-DMG.

2.5. Batch mode DLS & zeta potential

DLS and zeta potential measurements of RNA-LNPs were performed on a Zetasizer Nano ZS system (Malvern Panalytical). For size measurements, the LNPs were diluted 100x in sterile filtered PBS and measured at 20 °C. For zeta potential measurements, the particles were diluted 100x in sterile, filtered 10% PBS (PBS that was diluted 10x to not have too high salt concentrations). Five replicates per sample were performed. Zeta potential measurements were performed in a disposable folded capillary zeta cell (DTS1070, Malvern Panalytical), applying the standard operating procedure (SOP) developed by the EUNCL laboratory [37]. Average values obtained by cumulant analysis and PSD by intensity are reported in Table 1.

2.6. Nanoparticle tracking analysis

NTA measurements of the LNP1-RNA samples were performed on a NanoSight NS300 instrument (Malvern Panalytical). For size measurements, LNPs were diluted 30,000x in PBS. A 405 nm laser was used to visualise particles present in a given field of view. Three recordings of the laser interacting with particles were captured, each for 60 s, using an EM-CCD camera for each analysis. The camera level and focus were manually controlled and chosen by the operator (typical values: camera level 14, focus 0–60). The detection level was optimised by the operator (typical value of 4) and the recordings were subsequently analysed by the NanoSight 3.2 software to determine particle numbers per frame and sample concentrations. The reported value is the average of 3 measurements. Measured number-weighted distributions for all samples were averaged over repeated runs and the concentration in particles/mL/nm was plotted *vs* the hydrodynamic radius in histogram format with a bin size of 1 nm in order to be directly comparable with particle concentration calculated by AF4-MALS.

Table 1
Physical-chemical attributes of the LNP-RNA samples. Average and (standard deviation) values are reported. Rz = z-average hydrodynamic radius, PdI = Polydispersity index.

Physical-chemical attribute	LNP1-RNA batch#1	LNP2-RNA
Size by batch DLS	Rz = 75 (1) nm PdI = 0.07 (0,01)	Rz = 76 (1) nm PdI = 0.12 (0.01)
Zeta potential	−11 (1) mV	−2 (1) mV
Total lipid concentration	1.021 mg/mL	2.046 mg/mL
API loading	siRNA: 84 μg/mL	siRNA: 187 μg/mL

2.7. Asymmetric-flow field-flow fractionation measurements

Two widely available commercial platforms were used for this study: in Lab1, an AF2000 Multiflow FFF (Postnova Analytics) and in Lab2 an Eclipse AF4 (Wyatt Technology). All platforms included necessary isocratic pump(s), degasser, and autosampler injectors. Additionally, each system was equipped with a minimum of three online detectors relevant to the present work—MALS, UV–Vis absorbance and RI—from the corresponding AF4 vendor. The Eclipse AF4 was further equipped with a DLS detector integrated into the MALS instrument (WyattQELS, Wyatt Technology). The corresponding LC and FI fractionation channels from Wyatt Technology (Lab2) and from Postnova Analytics (Lab1) were tested. The elution profiles are reported in Fig. 2 (LC) and Fig. 4 (FI). Common conditions used in the analysis were: (i) sample injected volume: 20–50 μL of undiluted sample or of sample diluted by 2.5x (total injected mass: 8–50 μ); (ii) membrane: 10 kDa regenerated cellulose; (iii) mobile phase: isotonic PBS pH 7.4; (iv) spacer: 350 μm; (v) injection flow or tip flow (FI channel): 0.2 mL/min; (vi) detector flow: 0.5 mL/min. In standard AF4 mode, focusing was performed at either 0.75 mL/min (linear profile) or at 0.65 mL/min (exponential profile) for 9 min (optimized method) or less (2–9 min during method optimization). The optimised protocol derived in this work is described in detail in section S1.

Prior to the analysis, the membrane was conditioned by injecting 20 μL of BSA at 5 mg/mL and then the concentrated LNP samples (20 μL of undiluted or 2.5x diluted sample) until a constant recovery was obtained (typically after 3 repeated injections). The online MALS detectors were calibrated at a scattering angle of 90° and the remaining detector angles normalized to the response at 90° using an isotropic scatterer (e.g., bovine serum albumin monomeric form) according to manufacturer recommendations using the LC. As a quality control when using the FI, MD-AF4 performance was checked by injecting 20 μL of BSA at 0.5–1 mg/mL, which avoids channel overloading (Figure S1). Data analysis was performed with ASTRA 7.1.3 software (Wyatt Technology) or AF2000 ControlSuite software (Postnova Analytics).

2.7.1. Sample preparation for MD-AF4 analysis

A 20 μL aliquot of LNP-RNA suspension was injected either undiluted or diluted by 2.5x in PBS. For stability studies in physiological conditions, LNP1-RNA (batch #4) was incubated in PBS, or PBS + 10% FBS or PBS + 10% HS or in CSF for 24 h at 37 °C and then an aliquot injected into the MD-AF4 system.

2.7.2. Sample recovery

Sample recovery (R%) was calculated as indicated in ISO/TS 21,362 [22] by integrating the area under the UV–VIS peak for each sample eluted, with and without: (i) the applied XF (both for the standard LC and for the FI channels) and (ii) the focusing step (only applicable to the LC) [17]. The results with XF and/or focusing are compared to the results obtained without XF in order to calculate R%. Only the main peak (s) associated with particle elution was considered for the calculation of R%, while the areas under the void peak and under the release peak were excluded from the calculation and their R% values were estimated separately (*the release peak, also called retained peak, is a peak that contains material that is retained but not size separated, and which elutes only after crossflow ceases*). R% is considered acceptable if analyte loss from the main peak(s) is 30% or less.

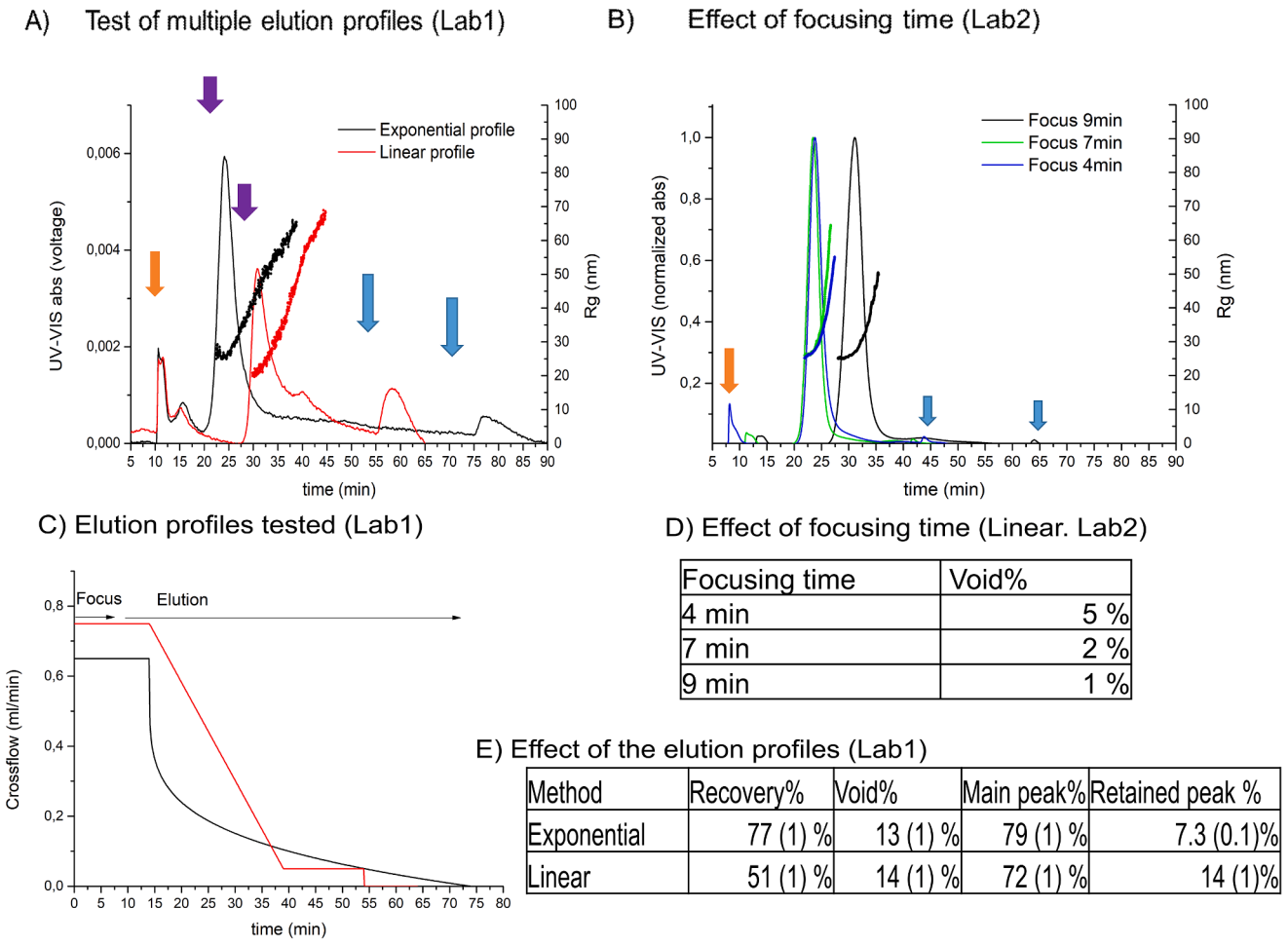

Focusing time	Void%
4 min	5 %
7 min	2 %
9 min	1 %

Method	Recovery%	Void%	Main peak%	Retained peak %
Exponential	77 (1) %	13 (1) %	79 (1) %	7.3 (0.1)%
Linear	51 (1) %	14 (1) %	72 (1) %	14 (1)%

Fig. 2. MD-AF4 results using the LC. A) UV fractograms of LNP1-RNA overlaid with R_g values, measured by Lab1 using the LC with two different XF profiles (linear and exponential) presented in figure C, showing (i) a large void peak (orange arrow), (ii) the main peak associated with NPs (violet arrow) and (iii) a large, retained peak (light blue arrow). ; B) UV fractograms of the same sample overlaid with R_g values, measured by Lab2 using the LC with the linearly decreasing XF profile of Figure C but with focusing times of 4, 7 and 9 min. C) XF profiles applied: exponential (black) and linear (red) decreases of the XF. D) Void peak height as % of the main peak for varying focus times with linear XF profile, Lab2. E) Retained peak height as % of the main peak for linear and exponential XF profiles, Lab1.

Sample recovery is a key indicator used for the evaluation of configurations tested during method optimization. Generally, the measurements of recovery were performed using UV detection by Lab 1 at 230 nm and by Lab 2 at 260 nm (figures reported in the main text). However, in the case of two specific batches, one of LNP1-RNA and one of LNP2-RNA, recovery was measured at both wavelengths with comparable results (Figure S2), demonstrating that both wavelengths can be used for calculating particle recovery. Notably, absorption at 230 nm is associated with the presence of both RNA and lipids, while absorption at 260 nm is associated mostly with RNA; no significant absorption from the lipid components is expected though the component of UV extinction due to scattering may result in a relatively low change in amplitude if lipid loss occurs. For this reason, we generally suggest checking recovery at 230 nm, as described in section S1.

2.7.3. Nanoparticle sizing by AF4-MALS-DLS:

To compare size values obtained using the different software packages provided by the two instrument manufacturers, the Berry model was applied to the analysis of MALS data, as suggested by [17]. Data reporting is performed according to ISO/TS 21362 [22]. The complete fractogram(s) of the eluted samples, showing R_g and the detector response(s) (UV–Vis and/or 90° light scattering intensity), are always reported. When Wyatt and Postnova results are compared on the same plot, UV–Vis or MALS detector signals are normalized. When data from a single laboratory are reported, detector voltage without normalization is preferentially shown.

The mode value of R_g (the peak maximum of the UV–Vis concentration signal), and the spread of R_g across the FWHM of the UV–Vis peak are also reported in tabular format. The average of R_g across the FWHM is not calculated, since due to the clear upward size trend across the LNP peak, the mean across the FWHM is not considered representative [22]. In the case of Lab2, the hydrodynamic radius was measured by the DLS detector positioned at 135° in the MALS read head, with autocorrelation functions analysed by the method of cumulants. As an indirect indicator of particle shape, the shape factor $\rho = R_g / R_h$ is calculated and reported as well.

2.7.4. Particle concentration measurements by AF4-MALS:

MALS data acquired with Wyatt instruments (Lab2) were further analysed to calculate particle concentration by means of ASTRA's 'number density' method, which requires knowledge of the particles' refractive index and shape. The output of the analysis provides the number of particles/mL in each data slice and the total number of particles in a selected peak region. The total particle concentration in the original aliquot is calculated by selecting a region covering all the eluting particles, obtaining the total number of eluting particles and dividing by the injected volume.

Particle refractive index for this analysis is calculated from the weight percent (w-%) of RNA and lipids, determined by LC-MS/MS and Ribogreen analysis (Table 1), and the refractive indices of RNA and

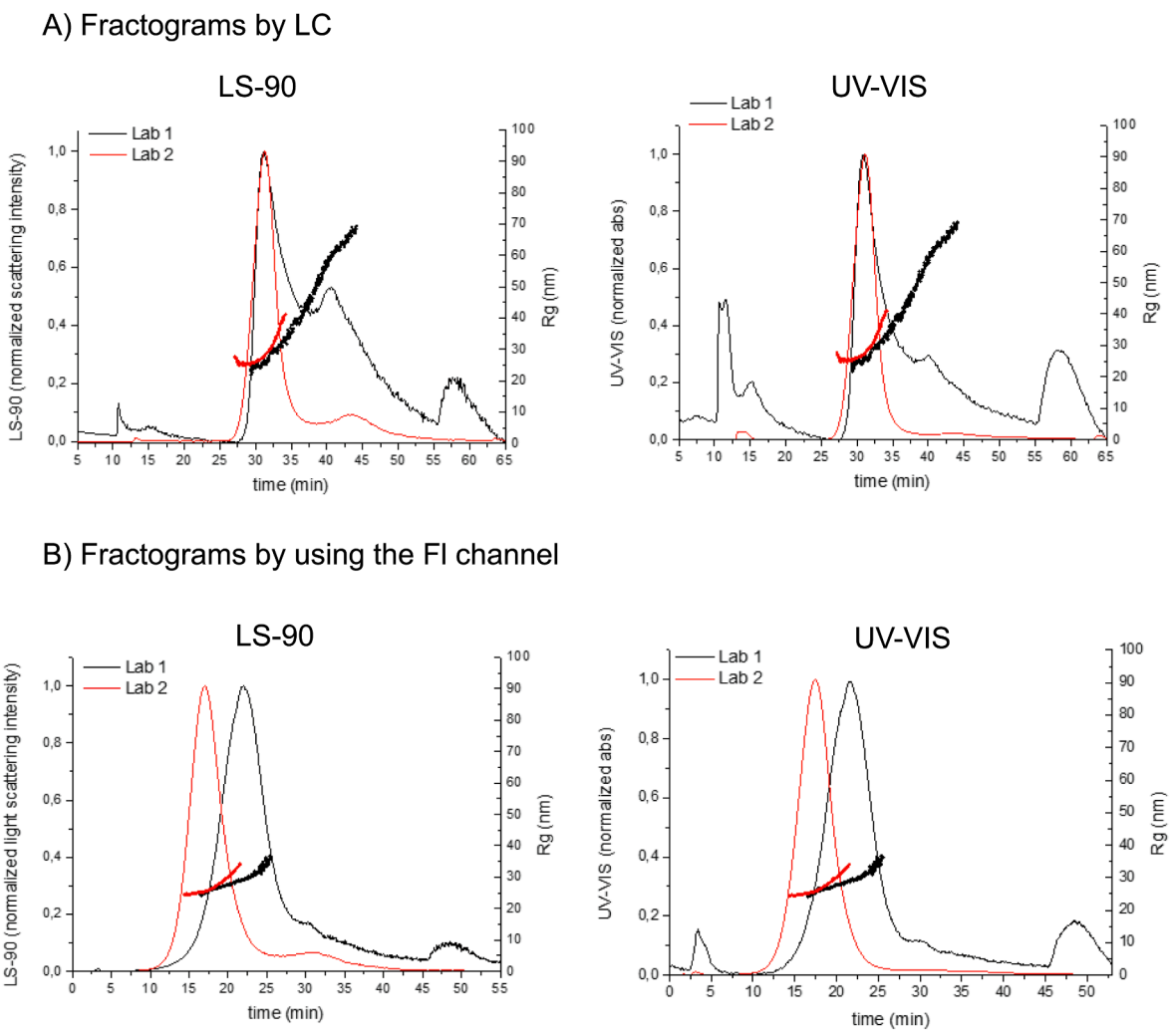

C) Tabular summary of the results

	LC-AF4			FI-AF4		
	R %	Rg mode (nm)	Rg Spread (nm)	R %	Rg mode	Rg Spread (nm)
Lab 1	51 (1)%	Peak 1 = 23 (2) Peak 2 = 57 (1)	na	84 (2)%	27 (1)	7 (1)
Lab2	91 (1)%	27.0 (0.5)	11 (2)	99 (1)%	26 (1)	6.5 (0.5)

Fig. 3. Comparison of the FI and LC AF4 methods. Fractograms obtained for LNP1-RNA by applying a linearly decreasing XF profile for Lab1 (black) and Lab 2 (red) using (A) the LC and (B) the FI channel. Light scattering intensity and UV–Vis absorption are reported on the left and right panels, respectively, together with the R_g profile estimated by Berry model. C) Summary of the results averaged over 3 measurements. Values in parentheses represent the standard deviation of the mean.

lipids. RI of each substance is calculated from partial specific volume ν and specific refractive index increment (dn/dc) values of the substance in the solvent at the wavelength of the MALS laser, 660 nm, as follows: $RI_{substance} = (dn/dc_{substance} / \nu_{analyte}) + RI_{solvent}$. The final calculation of particle refractive index (pRI) is as follows: $pRI_{LNP\text{-}RNA} = RI_{RNA} \times w\text{-}\%_{RNA}/100 + RI_{lipids} \times (1 - w\text{-}\%_{RNA}/100)$, where $RI_{RNA,\ 660\ nm} = 1.62$ and $RI_{lipids,\ 660\ nm} = 1.46$. Please note that a small variation of the RI will significantly impact the particle concentration results derived by light scattering data, and thus care should be taken to use the correct RI values for the analysis. The dependence of particle concentration on RNA fraction is reported in SectionS2. According to the data reported, a 10% change in RNA weight fraction, e.g., from 0.25 to 0.225, results in a 4.7% change in particle concentration.

For LNPs a spherical shape is assumed, and the MALS angular data were fit to a sphere model to determine the apparent geometric radius which is used to calculate particle concentration. In addition to slice-by-slice particle concentrations and total particles in a selected peak, ASTRA reports a PSD. The PSD calculated by the 'number density' method is currently reported by the ASTRA 7 software in relative units on a logarithmic size axis. We have developed a spreadsheet which transforms the PSD reported by the software in relative units into a number-based PSD in particles/mL/nm on a linear size axis. The Excel macro is available for the readers as Supplementary file#2 and detailed instructions for its use are provided in the supplementary section. The

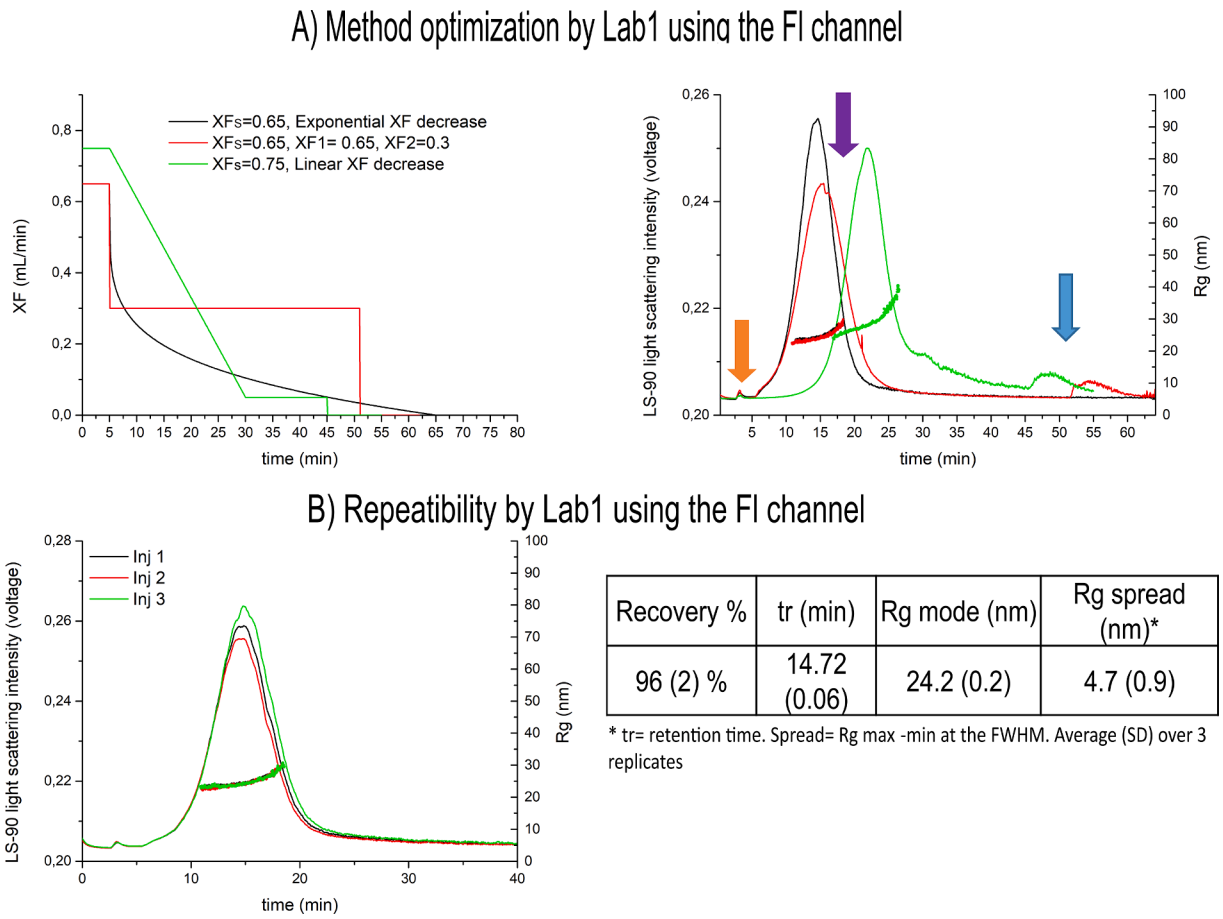

Recovery %	tr (min)	Rg mode (nm)	Rg spread (nm)*
96 (2) %	14.72 (0.06)	24.2 (0.2)	4.7 (0.9)

* tr= retention time. Spread= Rg max -min at the FWHM. Average (SD) over 3 replicates

Fig. 4. Method optimization and repeatability. A) Left: Exponentially (black) or linearly (green) decreasing crossflow (XF) profiles, and constant XF profile (red), used in method optimization performed by Lab1 using the FI channel. 'XFs' in the legend indicates starting XF value. Right: fractograms showing the light scattering intensity at 90° and Rg values obtained for each XF profile. B) Assessment of repeatability of the optimal method, consisting of the exponential XF profile. Left: LS fractograms; right: results and performance indicators, where values in parentheses indicate standard deviations.

PSD calculated for a bin size of 1 nm are reported in particles/mL/nm and compared with particle concentrations measured by NTA. The total particle concentration (particles/mL) was estimated by integrating the differential PSD obtained and verified to correspond to the total concentration reported by ASTRA's number density method for the entire fractogram.

3. Results and discussion

The basic physical–chemical characterisation of the LNP-RNA samples, including particle sizing with batch mode DLS, zeta potential measurements, total lipid quantification by LC-MS/MS and RNA loading by Ribogreen analysis, are summarized in Table 1. Size measured by DLS is comparable. The samples are both neutral (-10 mV < zeta potential < 10 mV), as typical for pegylated LNPs and of PEGylated liposomes. Despite the neutral values, steric interactions are determinant to guarantee particle stability, and therefore a neutral zeta potential is not an indication of particle instability. And vice versa, zeta potential values per se cannot be used to evaluate particle (in)stability, since the surface charge values are not significantly changing during particle aging (data not shown).

3.1. LNP-RNA recovery when separating with the standard AF4 channel is low

Initial MD-AF4 measurements of LNP1-RNA (Figure S3) followed the procedure reported by Caputo et al. [19] which uses the LC. Unlike the LNP formulations tested in the previous work, LNP1-RNA exhibited unacceptably low recovery (<70%). Moreover, the LNP-RNA fractograms exhibited a large void peak, presumably arising from particle destabilization during focusing, leading to the release of LNP components that absorb at 230 nm (mRNA, lipid or both). The quality of the results was very poor in comparison with measurements of doxorubicin liposomal formulations or solid lipid nanoparticles obtained on the same platform [7,9]. These preliminary results underscored the need for development of an LNP-RNA-specific MD-AF4 method. With this aim in mind and with the understanding that the issues encountered were likely caused by the AF4 focusing step, a method optimization study was launched. Two different instrument platforms were selected: Lab1 – MD-AF4 system from Postnova Analytics, Lab2 – MD-AF4 system from Wyatt Technology. In both labs, LC and FI channels were tested and compared to investigate if the FI channel option could improve performance and increase sample recovery.

The first critical point that emerged was that, independently of the platform and channel type, the membrane must be conditioned with 3–5 injections of the sample in order to reach stable recovery (Figure S4). Once this pre-requisite was established, the impact of focusing time in the LC configuration was investigated. The elution profiles used at this stage to test the effect of focusing are reported in Figure S5. It was demonstrated that, in order to increase sample recovery and reduce the initial void peak, focusing time should be relatively long: 7 – 9 min (Fig. 2C).

Notably, the LC method for LNP1-RNA was not fully reproducible and transferable between the two platforms. As shown in Fig. 2A and 2B

the same focusing conditions and subsequent linear XF profile produced significantly different results between Lab1 and Lab2 in terms of the elution profile and sample recovery. Recovery in Lab1 (51%) was significantly lower than in Lab2 (91%). Moreover, Lab 1 fractograms exhibited a much larger void peak (14%, *vs* 1% in Lab 2), and a significant retained peak (14%, *vs* nearly undetectable in Lab 2).

Finally, the presence of a second peak was evident in the 90° light scattering fractogram acquired by Lab1. The additional peak occurred at later elution time than the primary peak, with higher amplitude and particle sizes between 40 and 75 nm. This peak could only be explained as aggregates formed during focusing (i.e, artefacts). The latter peak was almost absent in the data from Lab2.

The difference between the results obtained by Lab1 and Lab2 with the LC configuration, analysing the same sample and applying the same method, is best explained by the different focusing mechanisms. The instrument tested in Lab 1 uses tip-injection focusing, while the CDI focusing/relaxation mode was used in Lab 2 [38] (Fig. 1). No such difference was found for robust lipid-based nanoparticles that are not sensitive to focusing, e.g. liposomal doxorubicin analysed by Parot et al. [17]. However, in the case of LNP1-RNA, our results indicate that the tip-injection design is more likely than the CDI design to destabilize particles. In tip-injection, the sample must migrate over the course of several minutes from the tip to the focusing zone. This could induce a higher shear and concentration stress on the sample, which would explain the stronger destabilisation (larger void peak) and the aggregate peak observed by Lab1.

3.2. The FI channel improves sample recovery to acceptable levels

All the evidence acquired on the LC by Lab1 pointed to the need to further optimize the MD-AF4 method. Simply changing the elution profile by reducing the FF from 0.75 to 0.65 mL/min and implementing a more gentle, exponential XF profile were not satisfactory.

As an alternative approach, the authors investigated the performance of the FI channel. As in the case of the LC, a fresh membrane had to be conditioned with 3 injections of the sample until stable recovery was observed. The linear XF profile tested in the LC configuration was transferred to the FI channel with the focusing step replaced by a sample injection step, keeping tip flow at 0.2 mL/min while applying XF of 0.75 mL/min; elution was initiated with a constant XF of 0.75 mL/min for 5 min before switching to the linearly decreasing ramp.

In Fig. 3, the UV–Vis and light scattering fractograms obtained with the FI channel are reported. The results are compared with the elution profile obtained by the standard LC channel using the same linear ramp. Recovery obtained by Lab 1 increased from 51% in the LC to over 84% in the FI channel, reaching an acceptable level (i.e., above 70%). Moreover, the void and the retained peaks experienced by Lab1 in the LC configuration are significantly decreased in percentage as seen in the UV–Vis fractograms in Fig. 3B, right panel. Similarly, the peak associated with particle aggregates detected by Lab1 almost disappeared upon using the FI channel, as seen in the LS fractogram in Fig. 3B, left panel.

The increase in sample recovery using the FI channel is associated with a slight decrease in resolution, exhibited as a slight increase of peak width, in agreement with previous studies [30]. However, the loss in resolution does not impact the quality of LNP1-RNA size measurements. Both the mode and spread of R_g measured by both platforms are comparable for the main particle peak, demonstrating the reproducibility of the method for size measurements across different platforms.

We thus conclude that the FI channel is a robust solution for the analysis of the LNP-RNA in both instrumental platforms tested. Reproducibility and transferability of the method were clearly demonstrated. The FI channel should be preferred over the LC for this application, especially in the case of the platform used by Lab1 which was subject to substantially poor recovery using the standard LC configuration.

3.3. Method optimization, precision, and repeatability of the FI channel

The FI-AF4 method described in the previous section fully satisfies the criteria presented in ISO/TS 21362 and in the SOP developed at the EUNCL [22,23,39]. However, even when using the FI channel, a void peak and a retained peak are observed in the elution profile measured by Lab1 but not by Lab2. As the final step of method optimization, the authors attempted to further optimize the XF profile in the instrumental configuration used by Lab1 in terms of sample recovery. As showed in Fig. 4A, three different elution profiles were tested: (i) Linearly decreasing XF profile starting from XF = 0.75 mL/min (same as tested in the previous section, shown in green in Fig. 4), (ii) Two constant XF steps, 0.65 and 0.3 mL/min (red plot in Fig. 4), and (iii) an exponential decrease starting from XF = 0.65 mL/min (black in Fig. 4). Not surprisingly, reducing the initial XF rate and imposing a fast reduction of XF via an exponential decay helps to further improve recovery. The best result for sample recovery was obtained with the exponentially decreasing XF profile: R% = 96% (exponential XF), 84% (linear XF) or 81% (constant XF). Moreover, the repeatability of the exponential XF profile tested by three replicated injections, (Fig. 4B) satisfied the requirements of ISO/TS 21362: the coefficient of variation (COV = standard deviation/mean) was less than 5% for all relevant parameters including sample recovery, retention time and the mode R_g. The exponential XF profile was therefore selected as the method of choice for further studies.

3.4. Assessment of batch-to-batch variability and formulation screening

Data quality in the MD-AF4 analysis using the FI channel is sufficient to investigate fine size changes in the LNP formulation, e.g., to detect batch-to-batch variability. Fig. 5A compares four batches of LNP1-RNA. While batch#1 and batch#2 do not show significant differences in retention time, R_g and polydispersity, batch#3 is markedly more polydisperse (higher spread) and batch#4 exhibits higher R_g values for the same elution time compared to the other batches.

Only a thorough assessment of safety and efficacy (in vitro/in vivo) would define if the size differences detected for this specific formulation (LNP1-RNA) are significant in terms of quality. Nevertheless, MD-AF4 is confirmed to be a very sensitive technique to detect small variations in physical properties in different batches. Similarly, small changes in the physical properties arising from modification of the chemical composition of LNPs can be investigated with MD-AF4. In Fig. 5B, we see that a different ionizable lipid (LNP2-RNA, where C12-200 replaces MC3) induces a shift of the PSD to larger sizes and increases sample polydispersity.

Interestingly, in cases of batch#4 (Fig. 5A) and LNP2-RNA (Fig. 5B), an increase in particle size R_g is not associated with a corresponding increase in retention time, which is usually related to the hydrodynamic size R_h. Two possibilities may be considered for this discrepancy: either the interaction chemistry between the particles and the membrane differ between samples (different particle surface chemistry or different membrane chemistry) or the particle shape is significantly different between the samples despite having the same R_h distribution (or both differences occur simultaneously). Further studies are ongoing to better investigate the particle structure and surface components by advanced structural analysis in order to gain a better understanding of differences in physical–chemical properties associated with the different batches or formulations. Nevertheless, the results shown in Fig. 5A and 5B demonstrate that MD-AF4 was able to detect a small but significant difference in size and polydispersity, while batch-mode DLS analysis of the same samples did not indicate any differences, a result of the low resolution of the latter technique (Table 1).

To conclude, our results confirm what has been previously demonstrated by many studies: adding an AF4 separation step before size analysis increases the measurement resolution and enables detection of fine changes in particle physical properties. Those size differences are

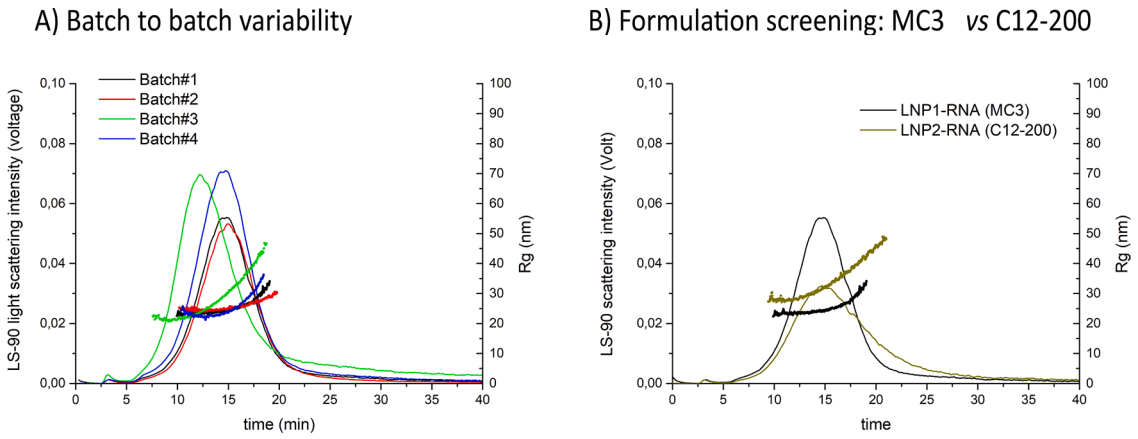

Fig. 5. Assessment of batch-to-batch variability and of modification of the chemical composition. A) LS fractograms overlaid with R_g values from four batches of LNP1-RNA; B) Comparison of LS fractograms and R_g values measured for LNP1-RNA and LNP2-RNA containing a different ionizable lipid (C12-200 *vs* MC3). Data shown here were measured by Lab1.

not detectable by batch DLS alone, due to its low resolution and the limited information provided [12,17,19,40]. AF4 separation combined with sizing analysis is therefore very useful for formulation screening, quality control and stability studies, both at the R&D stage and in the pharma setting. However, whether the differences detected by MD-AF4 in different batches do indicate compromised safety or efficacy, or are within the acceptable range, can only be determined by combining MD-AF4 measurements with evidence from detailed in-vitro/in-vivo screening.

3.5. Assessing stability during storage and in physiological media

As an example of the applicability to stability studies in simple media, the optimised FI-AF4 method was used to measure the stability of LNP1-RNA (Batch#1) during storage at 4 °C and room temperature (RT, 20 °C). As shown in Fig. 6A, the LNP1-RNA sample kept at RT for 4 weeks started to show signs of instability. Its fractogram (light blue curve) presents a tail of aggregates eluted after 20 min, indicating a change of the formulation during storage, while the sizing profile of the sample stored for 4 weeks at 4 °C is not statistically different from the particles measured at t_0.

A critical parameter for all NPhs, including LNP-RNA, is their stability in physiological conditions [41]. In fact, in biologically relevant media, LNP-RNA interacts with plasma proteins to modify their surface, e.g., induce formation of a protein corona. In the case of strong nanoparticle-protein interactions, the physical properties of nano-formulations may be significantly impacted, e.g., by agglomeration or particle dissolution phenomena. Such strong destabilization is not expected for an LNP-RNA like Onpattro, but it is known that the formation of the protein corona does impact critically the biodistribution properties. In fact, the adsorption of specific proteins such as apolipoprotein E (ApoE) on the LNP-RNA surface strongly favours liver accumulation [42].

MD-AF4 has been demonstrated to be a very powerful method to measure size changes induced by particle-protein interactions, thanks to the separation of free proteins from the analyte particles prior to sizing analysis. Its potential to measure changes in particle size in presence of plasma proteins has already been shown on liposomal samples [12,13,17] and solid lipid nanoparticles [19]. Here, we tested the developed FI method to measure the physical stability of LNP1-RNA (Batch#4) after incubation with FBS and HS diluted 10% (v/v) in buffered PBS (pH 7.4). Stability in aCSF was also evaluated, as a brain-mimicking medium. It should be noted that aCSF is protein-free. Before incubation at 37 °C for t_0, 1, 4, 24, 48, and 72 h (6 different timepoints), these dilutions were aliquoted such that for every measurement only one of the aliquots was used and the rest remained undisturbed. The results obtained after a 24 h incubation at 37 °C are reported in Fig. 6B, while additional timepoints are shown in Figure S6. No major instability was detected in any of the conditions tested, which excludes concern of major particle aggregation or destabilisation phenomena. This is, however, not surprising as a very similar formulation (Onpattro) has already been accepted into the clinic, where major aggregation in the circulation

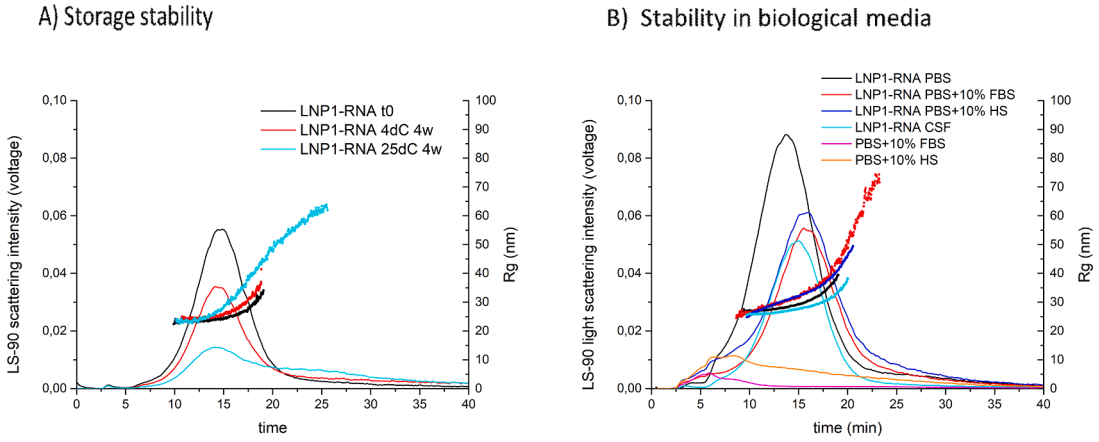

Fig. 6. LS fractograms overlaid with R_g values indicating A) stability of LNP1-RNA during storage during 4 weeks at 4 and 25 °C and B) stability of a different batch of LNP1-RNA in physiological media, measured after 24 h incubation at 37 °C in PBS, PBS + 10% FBS, PBS + 10% HS and CSF.

would be a major safety concern. Interestingly, in presence of serum proteins (10% FBS or HS), a shift of the retention time at later timepoints and an increase of the R_g mode of 4–6 nm are observed, indicating the formation of a protein corona (Table S5-S8). Finally, after 72 h (Figure S6), a reduction of size and an increase of the retention time are observed both in PBS and in PBS plus serum. This phenomenon may indicate a loss of PEG at long time points that could both reduce the size and at the same time induce stronger interaction between the particles and the membrane. We are currently evaluating the chemical stability in these conditions to confirm this hypothesis (paper under preparation).

We have demonstrated that the FI-AF4 separation method developed in this work can be used to study the formation of protein corona and changes of particle physical properties in biological media, responding to another important regulatory need. Our results are in line with findings reported in previous work by the EUNCL and of the NCI-NCL laboratories on both liposomal formulations and solid lipid nanoparticles [12,13,17,19]. In case particle instability is detected (which is not the case here) it would be important to correlate major changes in physical properties to safety concerns by associating MD-AF4 with in vitro and/or in vivo screening.

3.6. Not only sizing: Measurement of particle morphology and concentration by MD-AF4

In addition to the analysis of particle size distribution, MD-AF4 can be used for extended characterization applications, including: (i) change in nanoparticle size distribution after protein binding; (ii) molecular weight distributions of polymeric NP components; (iii) release of free coatings/surfactants (e.g. PEG) from the surface of the particles; (iv) investigation of drug loading; and (v) measurement of particle concentration [13,17,19]. As the last step of this work, we focused on the capability of MD-AF4 to measure two additional physical attributes of LNP-RNA and other lipid-based NPhs: particle morphology and particle concentration.

3.6.1. Particle morphology (shape factor)

The shape factor ρ, which is the ratio between R_g (determined by MALS) and R_h (determined by DLS), gives information about the particle morphology. For the main LNP1-RNA peak, a constant ρ value of 0.75 was calculated across the main particle peak (Fig. 7), as expected for a homogeneous and compact spherical particle, in agreement with cryo-TEM results previously reported for LNP-RNA formulations [21,43,44].

3.6.2. Particle concentration

For multiple applications, including vaccines, the quantitative PSD (particle/mL/nm) and the total particle concentration are critical attributes to be measured during development and for quality control purposes. In theory, with knowledge of particle size, shape, structure and of the RI of the particles and solvent, it is possible to transform the light scattering signal measured by MALS for each eluting volume fraction (slice) not only to a particle size but also to a particle concentration [US patent 6774994]. From there, one may further calculate the total particle number in any peak or segment, as well as the total particle number or concentration in the eluting sample. This calculation is implemented in the number density method of the ASTRA software, and has been used successfully for quite some time [14,45,46]. In addition to providing slice-by-slice particle numbers and integration over finite regions, the current version of the software, ASTRA 7.3.2, provides a contiguous number-based particle size distribution in relative units, with a logarithmic size axis and sub-nanometer binning. It is difficult to directly compare AF4-MALS concentration measurements with those obtained by single-particle techniques such as tunable resistive pulse sensing (TRPS) or NTA, typically expressed in absolute numbers over linear size axes and bins of 1 nm or more. Therefore, we have developed a macro to transform the relative PSD calculated by ASTRA software into a quantitative PSD in particle/mL/nm or particles/nm on a linear size axis with user-selectable binning (supplementary file#2). Details of the calculation may be found in the spreadsheet. The macro has already been tested on liposomes and polystyrene particles [35,36]. In this work, our aim was to test it on the LNP1-RNA formulation.

In Fig. 8, the results obtained by AF4-MALS measurement of LNP1-RNA are compared with NTA measurement of the same sample. NTA reports concentration *vs* the hydrodynamic radius, while the size reported by MALS when using the sphere model is the apparent geometric radius (R_g/0.77). The determined size may differ slightly from the hydrodynamic radius because the particle is not strictly homogeneous. In fact, the RNA in the core of the LNP-RNA nanoparticle has a higher RI than lipids, and this causes the apparent geometric radius to be slightly smaller than the hydrodynamic radius. In addition, NTA generally does not see low-contrast particles such as LNPs with radius smaller than ~25–30 nm, suggesting that a range of smaller particles detected by AF4-MALS is not detected by NTA, skewing the NTA mode to a higher average value [47]. Despite this, the results show close agreement in the size and particle concentration results obtained by the two techniques. The mode by MALS is 33 (±2) nm while the mode by NTA is 36 (±2) nm. Total concentration values of AF4-MALS are larger than those measured by NTA but less than a factor of two apart (possibly related to NTA missing the smaller particles). Nevertheless, the concentration measurements obtained could be considered rather close to each other, if the variability in concentration measurements performed by orthogonal analytical techniques (orthogonal = based on different physical principles) is considered [47].

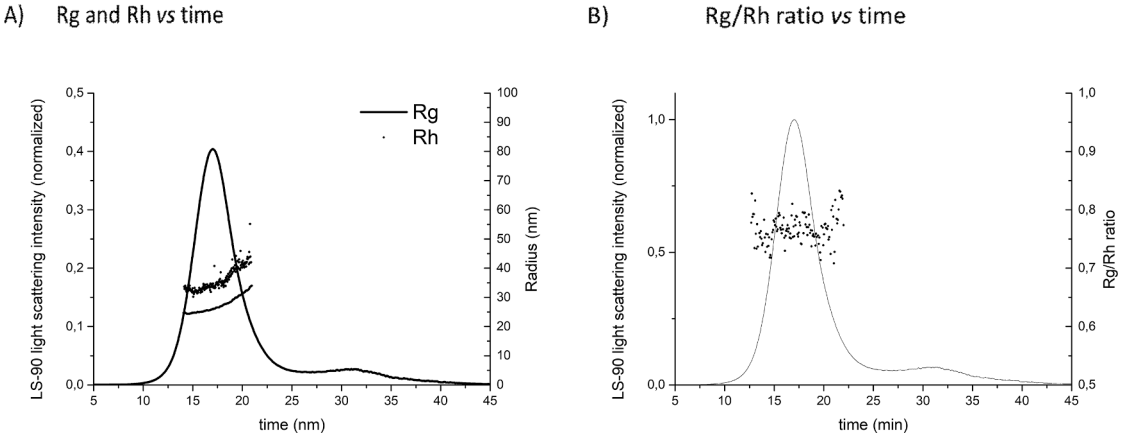

Fig. 7. LNP1-RNA particle morphology by MD-AF4. A) R_g and R_h profiles of LNP1-RNA measured by online DLS and online MALS; B) calculated R_g/R_h ratio across the peak.

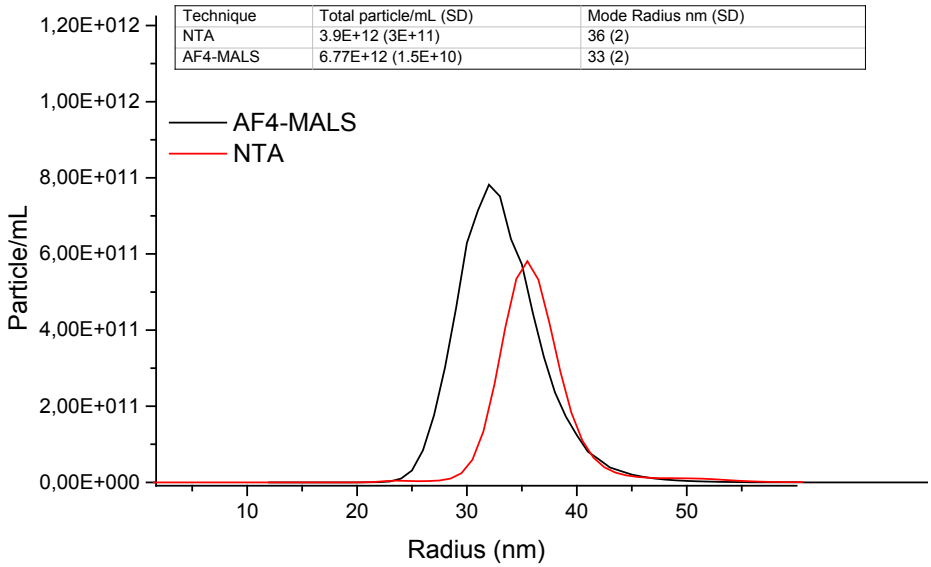

Fig. 8. Number-based particle size distribution (particle/mL/nm) obtained by NTA and by AF4-MALS. Total particle/mL concentration and mode of the radius are reported in the table in the graph. Values in parentheses indicate standard deviation of the mean calculated over 2 (AF4-MALS) or 3 (NTA) replicate measurements.

In the case of AF4-MALS, the RI is calculated from RI values tabulated for lipids and for nucleic acids, and the knowledge of the particle composition, as explained in the experimental section. It is important to note that, since the calculated concentration is proportional to the square of the difference between particle RI and solvent RI, if the particle RI value is in error then the final concentration values are affected. However, assuming the values for RI of pure RNA and pure lipids are accurate, errors in assigning the relative fractions do not lead to large concentration errors: a 3% uncertainty in the RNA weight fraction (for example, if the nominal weight fraction is 8% and the actual weight fraction is 11%) will lead to a 0.33% error in RI and corresponding 6.9% error in total particle number. At the same time, concentration values measured by NTA are affected by the definition of parameters such as the camera levels [35].

Concentration measurements are generally prone to large variability depending on experimental conditions and a golden standard does not exist at the moment. It is therefore always suggested to combine results obtained by complementary techniques. As shown here AF4-MALS is a viable option for samples of known optical properties, including LNP-RNA with known chemical composition, confirming what has already been proven for polystyrene, liposomes and virus-like particles [35,36].

4. Conclusions and future perspectives

In this work, thanks to an in-depth optimization effort, we have demonstrated a robust MD-AF4 protocol for analysing lipid-based nanoparticles for RNA delivery. In particular, we have shown that the use of a frit-inlet channel, available for most commercially available MD-AF4 platforms, enables measurement of size and physical stability of LNP-RNA with high reliability, reaching sample recovery above 90%. It is possible that previous studies were not successful because the MD-AF4 protocols developed for other lipid-based drug delivery systems, e.g., liposomes and solid lipid-based nanocarriers, are not directly applicable for RNA-LNP characterisation; sample aggregation and loss during focusing were experienced on one of the two platforms tested here. To our knowledge, this is the first work demonstrating the applicability of MD-AF4 for the analysis of PSD and particle concentration of lipid-based formulation for RNA delivery according to ISO/TS 21362 requirements.

In the frit-inlet configuration, MD-AF4 is confirmed to be a versatile technique to obtain information on the physical properties of NPhs such as LNP-RNA. At the early stages of product development, it can be used for formulation screening, providing robust and accurate understanding of the physical properties and stability of the products under evaluation. At later stages of product development, it could be a technique of choice for quality control in the pharmaceutical setting, relevant to batch-to-batch variability, lot release and other applications. Notably, we have shown that MD-AF4 can also provide information about particle concentration, with a comparable outcome to particle counting techniques such as NTA.

Method development for MD-AF4 could be time consuming and needs trained experts, differently from other techniques used to measure PSD and concentration like NTA or TRPS. However, when a method has been developed, it can be transferred and used routinely by analytical labs in pharmaceutical R&D and quality control, especially if they are familiar with standard chromatographic techniques. The additional information imparted by MD-AF4 relative to NTA or TRPS makes the effort worthwhile.

Further developments are underway by the AF4-MALS instrument providers for the characterisation of LNP-RNA and other nucleic acid delivery modes. For example, the lipid to nucleic acid ratio could be estimated by an advanced version of an algorithm originally developed for protein conjugate analysis, which combines the signal of MALS, UV and RI detectors. The novel approach is currently under evaluation and will be the subject of a follow-up paper. Particle separation by surface charge in addition to sizing is available in the electrical-AF4 (EAF4) technique and may be further exploited in the future to discriminate particles based on surface properties and charge in addition to sizing. Centrifugal FFF (CF3) can be used as a complementary separation mode, discriminating by size and density, so being able of separate loaded from unloaded particles.

Importantly, in the near future, software meeting GLP requirements will become available, to render MD-AF4 suitable for the pharmaceutical industry setting. With the advent of 21CFR(11)-compliant software, MD-AF4 will become a versatile analytical platform meeting regulatory needs for the characterisation of lipid-based nanopharmaceutical formulations for nucleic acid delivery, supporting regulators and other stakeholders in the upcoming nucleic acid revolution of the nanomedicine field.

Finally, the authors would like to stress that measurement of LNP-RNA physical properties and stability by MD-AF4 is only one of the many assessments needed during drug formulation development, in order to determine the CQAs of each specific formulation. In fact, as

mentioned by FDA [41], the nanomaterial's CQAs *should be determined with regard to its function and potential impact on product performance*. MD-AF4 evaluation of changes in physical properties due to formulation changes, batch-to-batch variability and/or changes in physiological environment should be paired with an exhaustive evaluation of safety and efficacy, toward an in-depth structure–function relationship analysis. Once the CQAs and their acceptable specifications have been determined for each specific formulation, MD-AF4 could also be also very useful in quality control to evaluate batch-to-batch variability of LNP-RNAs with very high resolution. With this work, the authors aim to make available to the community a reliable MD-AF4 method to be used during formulation screening and quality control of their LNP-RNA formulations. It is now their task to apply the MD-AF4 method developed here to specific formulations under development to determine their CQAs.

Author contribution

FC, RM and CJ designed the work. FC, RM, SH, JP and AH performed the experimental work. FC drafted the manuscript. DS developed the macro for particle concentration measurements used to analyse AF4-MALS data. All authors contributed to the manuscript revision. All the authors have approved the manuscript.

Declaration of Competing Interest

RM, DS and CJ are employees of Wyatt Technology and their contributions to this paper were made as part of their employment.

Acknowledgements

We thank Dr. Jeffrey D. Clogston for the suggestion of using the frit-inlet channel for LNP analysis and for the useful discussion during the writing of the paper. We thank Prof. Raymond Schiffelers - UMC Utrecht for providing the Dlin-MC3-DMA used in this work. FC, SH, JP, AH and SEB acknowledge the financial support from the European Commission under the H2020 programme under the grant refs # 761104 and # 721058.

Appendix A. Supplementary material

Supplementary data to this article can be found online at https://doi.org/10.1016/j.ejpb.2021.03.004.

References

[1] R.L. Setten, J.J. Rossi, S. Han, The current state and future directions of RNAi-based therapeutics, Nat. Rev. Drug. Discov. 18 (2019) 421–446, https://doi.org/10.1038/s41573-019-0017-4.

[2] M. Germain, F. Caputo, S. Metcalfe, G. Tosi, K. Spring, A.K.O. Åslund, A. Pottier, R. Schiffelers, A. Ceccaldi, R. Schmid, Delivering the power of nanomedicine to patients today, J. Control. Release 326 (2020) 164–171, https://doi.org/10.1016/j.jconrel.2020.07.007.

[3] P.S. Kowalski, A. Rudra, L. Miao, D.G. Anderson, Delivering the messenger: advances in technologies for therapeutic mRNA delivery, Mol. Ther. 27 (2019) 710–728, https://doi.org/10.1016/j.ymthe.2019.02.012.

[4] M.A. Oberli, A.M. Reichmuth, J.R. Dorkin, M.J. Mitchell, O.S. Fenton, A. Jaklenec, D.G. Anderson, R. Langer, D. Blankschtein, Lipid nanoparticle assisted mRNA delivery for potent cancer immunotherapy, Nano Lett. 17 (2017) 1326–1335, https://doi.org/10.1021/acs.nanolett.6b03329.

[5] J.A. Kulkarni, P.R. Cullis, R. van der Meel, Lipid nanoparticles enabling gene therapies: from concepts to clinical utility, Nucleic Acid Ther. 28 (2018) 146–157, https://doi.org/10.1089/nat.2018.0721.

[6] K.H. Moss, P. Popova, S.R. Hadrup, K. Astakhova, M. Taskova, Lipid nanoparticles for delivery of therapeutic RNA oligonucleotides, Mol. Pharmaceutics. 16 (2019) 2265–2277, https://doi.org/10.1021/acs.molpharmaceut.8b01290.

[7] I. Gómez-Aguado, J. Rodríguez-Castejón, M. Vicente-Pascual, A. Rodríguez-Gascón, M.Á. Solinís, A. del Pozo-Rodríguez, Nanomedicines to deliver mRNA: state of the art and future perspectives, Nanomaterials. 10 (2020) 364, https://doi.org/10.3390/nano10020364.

[8] A. Wadhwa, A. Aljabbari, A. Lokras, C. Foged, A. Thakur, Opportunities and challenges in the delivery of mRNA-based vaccines, Pharmaceutics. 12 (2020) 102, https://doi.org/10.3390/pharmaceutics12020102.

[9] M.D. Shin, S. Shukla, Y.H. Chung, V. Beiss, S.K. Chan, O.A. Ortega-Rivera, D. M. Wirth, A. Chen, M. Sack, J.K. Pokorski, N.F. Steinmetz, COVID-19 vaccine development and a potential nanomaterial path forward, Nat. Nanotechnol. 15 (2020) 646–655, https://doi.org/10.1038/s41565-020-0737-y.

[10] https://www.ema.europa.eu/en/documents/scientific-guideline/reflection-paper-data-requirements-intravenous-liposomal-products-developed-reference-innovator_en.pdf. Last access in October 2020.

[11] F. Caputo, J. Clogston, L. Calzolai, M. Rösslein, A. Prina-Mello, Measuring particle size distribution of nanoparticle enabled medicinal products, the joint view of EUNCL and NCI-NCL. A step by step approach combining orthogonal measurements with increasing complexity, J. Controlled Release 299 (2019) 31–43, https://doi.org/10.1016/j.jconrel.2019.02.030.

[12] S. Gioria, F. Caputo, P. Urbán, C.M. Maguire, S. Bremer-Hoffmann, A. Prina-Mello, L. Calzolai, D. Mehn, Are existing standard methods suitable for the evaluation of nanomedicines: some case studies, Nanomedicine. 13 (2018) 539–554, https://doi.org/10.2217/nnm-2017-0338.

[13] Y. Hu, R.M. Crist, J.D. Clogston, The utility of asymmetric flow field-flow fractionation for preclinical characterization of nanomedicines, Anal Bioanal Chem. 412 (2020) 425–438, https://doi.org/10.1007/s00216-019-02252-9.

[14] M. McEvoy, V. Razinkov, Z. Wei, J.R. Casas-Finet, G.I. Tous, M.A. Schenerman, Improved particle counting and size distribution determination of aggregated virus populations by asymmetric flow field-flow fractionation and multiangle light scattering techniques, Biotechnol. Progress. 27 (2011) 547–554, https://doi.org/10.1002/btpr.499.

[15] T. Bousse, D.A. Shore, C.S. Goldsmith, M.J. Hossain, Y. Jang, C.T. Davis, R. O. Donis, J. Stevens, Quantitation of influenza virus using field flow fractionation and multi-angle light scattering for quantifying influenza A particles, J. Virol. Methods 193 (2013) 589–596, https://doi.org/10.1016/j.jviromet.2013.07.026.

[16] J. Kuntsche, C. Decker, A. Fahr, Analysis of liposomes using asymmetrical flow field-flow fractionation: separation conditions and drug/lipid recovery: other Techniques, J. Sep. Science. 35 (2012) 1993–2001, https://doi.org/10.1002/jssc.201200143.

[17] J. Parot, F. Caputo, D. Mehn, V.A. Hackley, L. Calzolai, Physical characterization of liposomal drug formulations using multi-detector asymmetrical-flow field flow fractionation, J. Control. Release 320 (2020) 495–510, https://doi.org/10.1016/j.jconrel.2020.01.049.

[18] S. Hupfeld, H.H. Moen, D. Ausbacher, H. Haas, M. Brandl, Liposome fractionation and size analysis by asymmetrical flow field-flow fractionation/multi-angle light scattering: influence of ionic strength and osmotic pressure of the carrier liquid, Chem. Phys. Lipids 163 (2010) 141–147, https://doi.org/10.1016/j.chemphyslip.2009.10.009.

[19] F. Caputo, A. Arnould, M. Bacia, W.L. Ling, E. Rustique, I. Texier, A.P. Mello, A.-C. Couffin, Measuring particle size distribution by asymmetric flow field flow fractionation: A powerful method for the preclinical characterization of lipid-based nanoparticles, Mol. Pharmaceutics. 16 (2019) 756–767, https://doi.org/10.1021/acs.molpharmaceut.8b01033.

[20] J. Zhang, R.M. Haas, A.M. Leone, Polydispersity characterization of lipid nanoparticles for siRNA delivery using multiple detection size-exclusion chromatography, Anal. Chem. 84 (2012) 6088–6096, https://doi.org/10.1021/ac3007768.

[21] Y. Eygeris, S. Patel, A. Jozic, G. Sahay, Deconvoluting lipid nanoparticle structure for messenger RNA delivery, Nano Lett. 20 (2020) 4543–4549, https://doi.org/10.1021/acs.nanolett.0c01386.

[22] ISO/TS 21362:2018. Nanotechnologies — Analysis of nano-objects using asymmetrical-flow and centrifugal field-flow fractionation.

[23] EUNCL-PCC022: http://www.euncl.eu/about-us/assay-cascade/PDFs/PCC/EUNCL-PCC-022.pdf?m=1468937868. Last access in November 2020.

[24] F. Caputo, D. Mehn, J.D. Clogston, M. Rösslein, A. Prina-Mello, S.E. Borgos, S. Gioria, L. Calzolai, Asymmetric-flow field-flow fractionation for measuring particle size, drug loading and (in)stability of nanopharmaceuticals. The joint view of European Union Nanomedicine Characterization Laboratory and National Cancer Institute - Nanotechnology Characterization Laboratory, J. Chromatogr. A (2020) 461767, https://doi.org/10.1016/j.chroma.2020.461767.

[25] C. Contado, Field flow fractionation techniques to explore the "nano-world", Anal Bioanal Chem. 409 (2017) 2501–2518, https://doi.org/10.1007/s00216-017-0180-6.

[26] A. Zattoni, B. Roda, F. Borghi, V. Marassi, P. Reschiglian, Flow field-flow fractionation for the analysis of nanoparticles used in drug delivery, J. Pharm. Biomed. Anal. 87 (2014) 53–61, https://doi.org/10.1016/j.jpba.2013.08.018.

[27] A. Hinna, F. Steiniger, S. Hupfeld, M. Brandl, J. Kuntsche, Asymmetrical flow field-flow fractionation with on-line detection for drug transfer studies: a feasibility study, Anal Bioanal Chem. 406 (2014) 7827–7839, https://doi.org/10.1007/s00216-014-7643-9.

[28] A.-R. Jochem, G.N. Ankah, L.-A. Meyer, S. Elsenberg, C. Johann, T. Kraus, Colloidal mechanisms of gold nanoparticle loss in asymmetric flow field-flow fractionation, Anal. Chem. 88 (2016) 10065–10073, https://doi.org/10.1021/acs.analchem.6b02397.

[29] M. Ali, E. Hwang, I.-H. Cho, M.H. Moon, Characterization of sodium hyaluronate blends using frit inlet asymmetrical flow field-flow fractionation and multiangle light scattering, Anal Bioanal Chem. 402 (2012) 1269–1276, https://doi.org/10.1007/s00216-011-5531-0.

[30] C. Fuentes, J. Choi, C. Zielke, J.M. Peñarrieta, S. Lee, L. Nilsson, Comparison between conventional and frit-inlet channels in separation of biopolymers by asymmetric flow field-flow fractionation, Analyst. 144 (2019) 4559–4568, https://doi.org/10.1039/C9AN00466A.

[31] M.H. Moon, D. Kang, J. Jung, J. Kim, Separation of carbon nanotubes by frit inlet asymmetrical flow field-flow fractionation, J. Sep. Science. 27 (2004) 710–717, https://doi.org/10.1002/jssc.200401743.
[32] M.H. Moon, P.S. Williams, H. Kwon, Retention and efficiency in frit-inlet asymmetrical flow field-flow fractionation, Anal. Chem. 71 (1999) 2657–2666, https://doi.org/10.1021/ac990040p.
[33] U. Till, M. Gaucher, B. Amouroux, S. Gineste, B. Lonetti, J.-D. Marty, C. Mingotaud, C.R.M. Bria, S.K.R. Williams, F. Violleau, A.-F. Mingotaud, Frit inlet field-flow fractionation techniques for the characterization of polyion complex self-assemblies, J. Chromatogr. A 1481 (2017) 101–110, https://doi.org/10.1016/j.chroma.2016.12.050.
[34] WP2611- Application note: Characterization-of-nano-pharmaceuticals-with-FFF-MALS-DLS. https://wyattfiles.s3-us-west-2.amazonaws.com/literature/white-papers/WP2611-Characterization-of-nano-pharmaceuticals-with-FFF-MALS-DLS.pdf. Last access in October 2020.
[35] R. Vogel, J. Savage, J. Muzard, G.D. Camera, G. Vella, A. Law, M. Marchioni, D. Mehn, O. Geiss, B. Peacock, D. Aubert, L. Calzolai, F. Caputo, A. Prina-Mello, Measuring particle concentration of multimodal synthetic reference materials and extracellular vesicles with orthogonal techniques: Who is up to the challenge? J. Extracellular Vesic. 10 (2021) https://doi.org/10.1002/jev2.12052.
[36] F. Caputo, R. Vogel, J. Savage, G. Vella, A. Law, G. Della Camera, G. Hannon, B. Peacock, D. Mehn, J. Ponti, O. Geiss, D. Aubert, A. Prina-Mello, L. Calzolai, Measuring particle size distribution and mass concentration of nanoplastics and microplastics: addressing some analytical challenges in the sub-micron size range, J. Colloid Interface Sci. 588 (2021) 401–417, https://doi.org/10.1016/j.jcis.2020.12.039.
[37] F. Caputo, Zeta potential determination of nanoparticles in aqueous dispersions by PALS, http://www.euncl.eu/about-us/assay-cascade/PDFs/Prescreening/EUNCL-PCC-002.pdf?m=1468937877& (Last access in March 2021).
[38] Application of an asymmetrical flow field-flow fractionation channel to the separation and characterization of proteins, plasmids, plasmid fragments, polysaccharides and unicellular algae, Journal of Chromatography A. 461 (1989) 73–87. https://doi.org/10.1016/S0021-9673(00)94276-6.
[39] F. Caputo, D. Mehn, J.D. Clogston, M. Rösslein, A. Prina-Mello, S.E. Borgos, S. Gioria, L. Calzolai, Asymmetric-flow field-flow fractionation for measuring particle size, drug loading and (in)stability of nanopharmaceuticals. The joint view of European Union Nanomedicine Characterization Laboratory and National Cancer Institute - Nanotechnology Characterization Laboratory, Journal of Chromatography A. 1635 (2021) 461767. https://doi.org/10.1016/j.chroma.2020.461767.
[40] D. Mehn, F. Caputo, M. Rösslein, L. Calzolai, F. Saint-Antonin, T. Courant, P. Wick, D. Gilliland, Larger or more? Nanoparticle characterisation methods for recognition of dimers, RSC Adv. 7 (2017) 27747–27754, https://doi.org/10.1039/C7RA02432K.
[41] https://www.fda.gov/regulatory-information/search-fda-guidance-documents/drug-products-including-biological-products-contain-nanomaterials-guidance-industry. Last access in October 2020.
[42] V. Francia, R.M. Schiffelers, P.R. Cullis, D. Witzigmann, The biomolecular corona of lipid nanoparticles for gene therapy, Bioconjugate Chem. 31 (2020) 2046–2059, https://doi.org/10.1021/acs.bioconjchem.0c00366.
[43] J.A. Kulkarni, M.M. Darjuan, J.E. Mercer, S. Chen, R. van der Meel, J.L. Thewalt, Y. Y.C. Tam, P.R. Cullis, On the formation and morphology of lipid nanoparticles containing ionizable cationic lipids and siRNA, ACS Nano 12 (2018) 4787–4795, https://doi.org/10.1021/acsnano.8b01516.
[44] J.A. Kulkarni, D. Witzigmann, J. Leung, Y.Y.C. Tam, P.R. Cullis, On the role of helper lipids in lipid nanoparticle formulations of siRNA, Nanoscale. 11 (2019) 21733–21739, https://doi.org/10.1039/C9NR09347H.
[45] K. Eskelin, M.M. Poranen, H.M. Oksanen, Asymmetrical flow field-flow fractionation on virus and virus-like particle applications, Microorganisms. 7 (2019) 555, https://doi.org/10.3390/microorganisms7110555.
[46] Y.P. Chuan, Y.Y. Fan, L. Lua, A.P.J. Middelberg, Quantitative analysis of virus-like particle size and distribution by field-flow fractionation, Biotechnol. Bioeng. 99 (2008) 1425–1433, https://doi.org/10.1002/bit.21710.
[47] E.J. Petersen, A.R.M. Bustos, B. Toman, M.E. Johnson, M. Ellefson, G.C. Caceres, A. L. Neuer, Q. Chan, J.W. Kemling, B. Mader, K. Murphy, M. Roesslein, Determining what really counts: modeling and measuring nanoparticle number concentrations, Environ. Sci.: Nano. 6 (2019) 2876–2896, https://doi.org/10.1039/C9EN00462A.